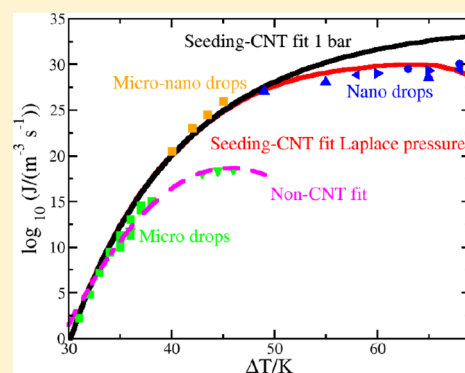


Homogeneous Ice Nucleation Rate in Water Droplets

Jorge R. Espinosa, Carlos Vega, and Eduardo Sanz*¹

Departamento de Química Física I, Facultad de Ciencias Químicas, Universidad Complutense de Madrid, 28040 Madrid, Spain

ABSTRACT: To predict the radiative forcing of clouds, it is necessary to know the rate at which ice homogeneously nucleates in supercooled water. Such a rate is often measured in drops to avoid the presence of impurities. At large supercooling, small (nanoscopic) drops must be used to prevent simultaneous nucleation events. The pressure inside such drops is larger than the atmospheric one by virtue of the Laplace equation. In this work, we take into account such pressure rise to predict the nucleation rate in droplets using the TIP4P/Ice water model. We start from a recent estimate of the maximum drop size that can be used at each supercooling, avoiding simultaneous nucleation events [Espinosa et al. *J. Chem. Phys.*, 2016]. We then evaluate the pressure inside the drops with the Laplace equation. Finally, we obtain the rate as a function of the supercooling by interpolating our previous results for 1 and 2000 bar [Espinosa et al. *Phys. Rev. Lett.* 2016] using the classical nucleation theory expression for the rate. This requires, in turn, interpolating the ice–water interfacial free energy and chemical potential difference. The TIP4P/Ice rate curve thus obtained is in good agreement with most droplet-based experiments. In particular, we find good agreement with measurements performed using nanoscopic drops, which are currently under debate. The successful comparison between the model and experiments suggests that TIP4P/Ice is a reliable model to study the water-to-ice transition and that the classical nucleation theory is a good framework to understand it.



To make climate change predictions, it is necessary to estimate the radiative forcing (the balance between absorbed and reflected solar radiation) caused by different factors. According to reports by the Intergovernmental Panel on Climate Change (IPCC), there are large uncertainties in the radiative forcing caused by clouds. Such uncertainty is partly due to the lack of reliable predictions of the ice content in clouds.^{1–3} These predictions rely on estimates of the ice nucleation rate, J , or the number of ice embryos that proliferate per unit time and volume.^{1–3}

In this paper, we focus on the rate of homogeneous ice nucleation from pure water, J_{hom} . Although ice formation in the atmosphere is thought to occur predominantly heterogeneously from aqueous solutions,^{1,4} the fact that clouds have been observed to supercool to very low temperatures (even below -35 °C)^{5–8} suggests that there is homogeneous ice nucleation from nearly pure water in clean atmospheric conditions (upper troposphere). Moreover, ice nucleation from solutions and heterogeneous ice nucleation are often treated as sophistication of the case of homogeneous ice nucleation from pure water.^{9–11} It is therefore relevant to fully understand and characterize the latter. Of course, predicting the freezing of clouds requires knowledge not only of the nucleation stage but also of the growth one. However, both the freezing stages are sufficiently complex so as to deserve separate attention.

Experiments to measure J_{hom} typically use suspended droplets ranging from microscopic to nanoscopic size to avoid heterogeneous ice nucleation on impurities. In Figure 1, J_{hom} measurements as a function of the supercooling ΔT —the

melting temperature minus temperature of interest—are reported. Green and blue symbols correspond to measurements performed with microscopic^{12–20} and nanoscopic^{21–24} droplets, respectively, whereas orange ones²⁵ correspond to droplet sizes in between both the ranges. Recent measurements from 2015,²⁶ downward green triangles, inspired in 2016 a new fit to J_{hom} (dashed pink curve²⁷) that shows a maximum at $\Delta T \approx 46$ K. Such a fit strongly clashes with measurements performed using nanoscopic drops at deep supercooling (blue points).^{21–24} According to these experiments, J_{hom} monotonously increases with supercooling, at least up to $\Delta T = 70$ K. Clarifying such discrepancy is a very relevant issue to atmospheric and climate science for the reasons explained in the previous paragraph. Several hypotheses have been put forward to explain the discrepancy.²⁶ A plausible one is a spurious overestimation of the rate in nanoscopic drops due to nucleation at the air–water interface, but this remains a controversial issue.²⁸

In a recent work, we have used TIP4P/Ice, a simple yet realistic water model,²⁹ to predict J_{hom} with computer simulations^{30,31} using the seeding³² and the mold integration techniques.³³ Our results for 1 bar, shown with a black curve in the figure, are in better agreement with the scenario supported by the nanoscopic drop measurements. In ref 30, we argue that the measurements corresponding to the downward triangles could be underestimated because the employed drops may be

Received: May 20, 2018

Revised: September 7, 2018

Published: September 27, 2018

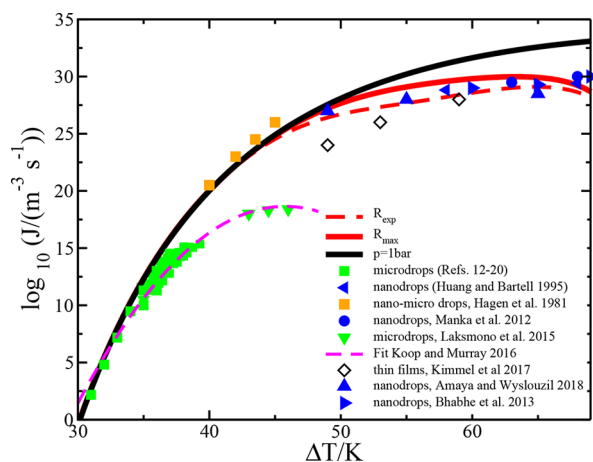


Figure 1. Ice nucleation rates as a function of supercooling, ΔT (difference between the melting temperature and temperature of interest). Solid symbols correspond to experimental measurements in drops. Green squares correspond to micron-sized drops from refs.^{12,20} downward green triangles are also micron-sized drops but are from ref 26, blue symbols correspond to nanoscopic drops,^{21–24} and orange symbols correspond to drops in between the nanoscopic and the microscopic regime.²⁵ Empty symbols correspond to measurements of the nucleation rate in thin films.³⁴ The dashed pink curve is a fit proposed in ref 27 and inspired by the publication of the data represented by the downward green triangles. Black and red curves correspond to simulation estimates using the TIP4P/Ice water model obtained with seeding.³² The black line corresponds to the rate estimate at 1 bar (from ref 30). In the red curves (this work) the effect of the Laplace pressure inside the drops is taken into account in the simulation rate estimate. The solid red curve corresponds to the rate measured in the largest possible drop where there is a single nucleation event, whereas the dashed red curve corresponds to the rate in drops of size typically used in experiments.

too large and contain many ice nuclei growing simultaneously. Then, the time needed to observe water freezing would no longer be limited by the nucleation stage, but rather by the time required for the nucleated ice embryos to grow and fill a fraction of the drop volume that enables freezing detection. Because the rate is determined under the expectation that only one ice cluster nucleates in each drop,²⁶ multiple nucleation events would lead to an underestimation of the nucleation rate. This multiple nucleation aggravates as the supercooling increases because J_{hom} goes up with ΔT . In Figure 2a, we reproduce our results from ref 30, where by combining simulation estimates of J_{hom} and that of the speed of ice

growth, we predicted $R_{\text{max}}(\Delta T)$, the maximum droplet radius that enables staying in the regime where drops are observed to freeze at the time required to nucleate a single critical ice cluster. As expected, R_{max} goes down with ΔT . Symbols shown in Figure 2a have the same legend as those shown in Figure 1. Downward triangles, that inspired the dashed pink fit in Figure 1 lie, in the region where our simulations predict that many ice clusters will simultaneously grow in the droplet.

We can now use $R_{\text{max}}(\Delta T)$ in conjunction with the Laplace equation, $\Delta P = 2\gamma_{\text{lv}}/R_{\text{max}}$ to estimate the pressure inside the largest drops that can be used if simultaneous nucleation events are to be avoided (γ_{lv} is the liquid–vapor surface tension). To do such an estimate, we have used the γ_{lv} temperature dependence given in ref 35, which we linearly extrapolated outside the reported measurement range (below $-25\text{ }^{\circ}\text{C}$). The smooth variation of γ_{lv} with temperature justifies such extrapolation. Using γ_{lv} for a flat interface could be inappropriate when dealing with curved drop surfaces. However, using a Tolman length of 1 \AA —larger than the values typically reported^{36–38}—to correct for curvature effects only yields changes of less than 2 mN/m for the smallest drops considered. We therefore neglect any curvature effects in γ_{lv} . The results for the pressure inside the drops as a function of the corresponding supercooling are shown in Figure 2b, indicated by the solid curve. For supercooling larger than $\sim 50\text{ K}$, the pressure sharply goes up. Therefore, rate measurements using drops can no longer be performed at 1 bar for $\Delta T > 50\text{ K}$, which is an interesting conclusion of our analysis. This has to be taken into account when comparing simulation estimates with droplet-based experimental measurements of the nucleation rate. This issue has been disregarded in the black curve shown in Figure 1, which entirely corresponds to 1 bar (in simulations, the rate is not computed inside the drops but in the bulk, thanks to periodic boundary conditions). The main aim of this paper is to provide a simulation prediction of $J_{\text{hom}}(\Delta T)$ that can be directly compared with drop-based measurements. This has been recently attempted in an experimental work, but only rough estimates were provided.²⁴

To achieve this goal, one needs to compute for each ΔT the rate at the pressure given by $p(\Delta T)$ in Figure 2. We have recently published J_{hom} at 1 and 2000 bar for TIP4P/Ice.³¹ Here, we interpolate our results to obtain J_{hom} at the desired pressure. We compute J_{hom} by plugging parameters obtained by simulations into the expressions given by the classical nucleation theory (CNT),^{39–42} a combination we call seeding.³² The CNT rate is given by

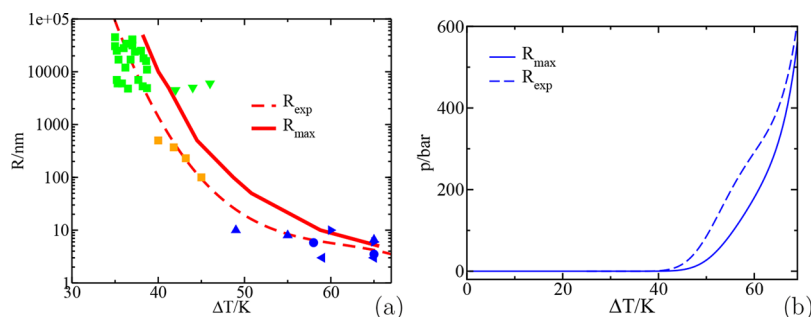


Figure 2. (a) Droplet radius as a function of the supercooling. The solid red curve corresponds to the maximum radius that enables measuring ice nucleation rates avoiding the simultaneous growth of several nuclei, R_{max} .³⁰ The red-dashed curve, R_{exp} , corresponds to a fit to the experimental data, excluding those given by downward green triangles. Symbols correspond to the experiments indicated in the legend of Figure 1. (b) Solid (dashed) corresponds to Laplace pressure inside drops of radius R_{max} (R_{exp}) as a function of the supercooling.

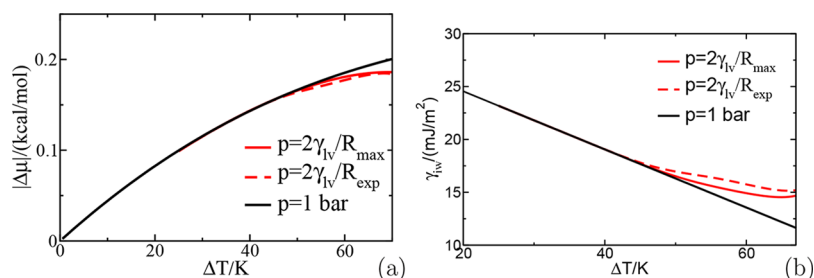


Figure 3. TIP4P/Ice water model predictions for the chemical potential difference between water and ice, (a), and the ice–water interfacial free energy, (b), as a function of supercooling. Black curves correspond to 1 bar,³⁰ the solid red curve corresponds to the largest drops that can be used while avoiding simultaneous nucleation events, and the dashed red curve corresponds to drops with sizes typically used in the experiments. To parametrize the nucleation rate we use the following fits for the red solid curves: $|\Delta\mu| = 0.0012522 + 0.0044213\Delta T - 1.6401 \times 10^{-5}\Delta T^2 - 1.259 \times 10^{-7}\Delta T^3$ and $\gamma_{iw} = 30.157 - 0.3219\Delta T + 0.0042643\Delta T^2 - 0.0001333\Delta T^3 + 1.3504 \times 10^{-6}\Delta T^4$, and these fits are for the red-dashed ones: $|\Delta\mu| = 0.00035032 + 0.0046013\Delta T - 2.3187 \times 10^{-5}\Delta T^2 - 6.9536 \times 10^{-8}\Delta T^3$ and $\gamma_{iw} = 29.986 - 0.25559\Delta T - 0.0010465\Delta T^2 + 4.6503 \times 10^{-6}\Delta T^3 + 2.9065 \times 10^{-7}\Delta T^4$.

$$J_{\text{hom}} = A \exp\left(-\frac{C\gamma_{iw}^3}{k_B T \rho_s^2 |\Delta\mu|^2}\right) \quad (1)$$

where C is a constant that depends on the shape of the critical nucleus (here, $16\pi/3$ for spherical clusters), A is a kinetic prefactor, k_B is the Boltzmann constant, ρ_s is the solid density, γ_{iw} is the ice–water interfacial free energy, and $|\Delta\mu|$ is the chemical potential difference between the bulk water and ice phases. $|\Delta\mu|$ is computed with thermodynamic integration^{30,43} and γ_{iw} with mold integration³³ and seeding³² for coexistence⁴⁴ and supercooled conditions,^{30,45} respectively. The γ_{iw} thus obtained has proven to give correct values for the nucleation rate when combined with the CNT.³² Therefore, the γ_{iw} we use for spherical critical clusters at supercooled conditions implicitly includes curvature and temperature corrections to that of a flat interface at coexistence.

As shown in Figure 3 of ref 31, neither A nor the solid density significantly change with pressure. Therefore, we use the values of A and ρ_s corresponding to 1 bar for any supercooling. To parametrize the rate, we use the following fits for A and ρ_s : $\ln(A/(\text{m}^{-3} \text{s}^{-1})) = 91.656 - 0.11729\Delta T - 0.00081401\Delta T^2$, $\rho_s/(\text{g}/\text{cm}^3) = 0.906 + 0.14 \times 10^{-3}\Delta T$.

The chemical potential difference can be easily obtained by thermodynamic integration from coexistence.^{46,47} In ref 31, we showed that $|\Delta\mu|$ does not strongly change from 1 to 2000 bar. The smooth variation of $|\Delta\mu|$ with pressure enables us to obtain it by interpolation at the required pressure for each supercooling. The results are shown in Figure 3a, where we compare $\Delta\mu(\Delta T)$ at 1 bar (the black curve) with that at the pressure given by $p(\Delta T)$ in Figure 2b (red solid curve). Both curves are obviously the same up to $\Delta T \approx 50$ K where, according to Figure 2b, the pressure inside the drops is the atmospheric one. Beyond that supercooling $|\Delta\mu|$ is lower for the drops, which will contribute to lower J_{hom} with respect to the 1 bar value ($|\Delta\mu|$ goes in the denominator of the exponential in eq 1).

We can also interpolate γ_{iw} between our previously published values for 1 and 2000 bar.³¹ The results are shown in Figure 3b (solid red curve). Again, there is a noticeable effect at large supercooling: γ_{iw} increases because of the fact that, in virtue of the Laplace equation, the pressure inside the drops exceeds the atmospheric one (as we have recently shown,³¹ the ice–water interfacial free energy increases with pressure). From eq 1, it is clear that an increase of γ_{iw} entails a decrease of the nucleation rate.

Then, both $|\Delta\mu|$ and γ_{iw} contribute to lower the nucleation rate inside the drops. With eq 1, the red curves in Figure 3 and the kinetic prefactor previously obtained,³¹ we can correct the black curve in Figure 1 to account for Laplace pressure effects. The result is the solid red curve in Figure 1, which is now in very good agreement with nanoscopic drop data (blue symbols). In fact, the red curve is in good agreement with all drop-based rate measurements (solid symbols in Figure 1) except from those that inspired the fit with a maximum at $\Delta T = 46$ K (dashed pink). To obtain the solid red curve in Figure 1, one needs to combine in eq 1 the fits to the solid red curves of $\Delta\mu$ and γ_{iw} given in the caption to Figure 3 with those to A and ρ_s given above.

The solid red curve in Figure 1 corresponds to the nucleation rate in the largest possible drop that can be used for each supercooling, avoiding multiple nucleation events (one with radius $R_{\max}(\Delta T)$). However, the droplets employed in experiments need not be of radius R_{\max} . In fact, in Figure 2a, one can see that the experimental droplet sizes typically lie below R_{\max} . It is, therefore, interesting to compute the nucleation rate for the droplet sizes typically used in the experiments, given by radius R_{exp} . We estimate $R_{\text{exp}}(\Delta T)$ by fitting the experimental values given in Figure 2a, excluding the downward green triangles because they lie in the multiple nucleation event region. The $R_{\text{exp}}(\Delta T)$ fit is given by the dashed red curve in the figure. Given that $R_{\text{exp}} < R_{\max}$, the pressure inside drops of radius R_{exp} is larger than that inside drops of radius R_{\max} (see Figure 2b). In fact, as shown in Figure 2b, now the pressure departs from the atmospheric one at milder supercooling, $\Delta T = 45$ instead of 50 K. Because a larger pressure causes a lower nucleation rate,^{31,48} the red dashed curve in Figure 1, corresponding to R_{exp} , lies below the solid red one, corresponding to drops with radius R_{\max} . In fact, the R_{\max} curve in Figure 1 is an estimate of the highest possible rate that can be measured using drops and avoiding multiple nucleation events. The R_{exp} curve in Figure 1 fits the experiments even better than the R_{\max} one, which further supports the reliability of the predictions given by our model. To obtain the dashed red curve in Figure 1, one needs to combine in eq 1 the fits to the dashed red curves of $\Delta\mu$ and γ_{iw} given in the caption to Figure 3 with those to A and ρ_s given above.

The experiments with thin films³⁴ (empty diamonds in Figure 1) are carried out at atmospheric pressure (with a flat air–water interface). Therefore, they should be compared with

the simulation predictions for 1 bar, as indicated by the black line in Figure 1. The comparison is not entirely satisfactory, and further work is required to clarify this issue. Furthermore, the comparison of thin-film experiments with droplet experiments in a supercooling regime where drops are expected to be at nearly atmospheric pressure ($\Delta T < 45$ K) does not look satisfactory either (as discussed in this work, for supercooling larger than 50 K thin film and droplet experiments cannot be compared because the latter are carried out at a higher pressure).

In summary, we have recently argued that there is a maximum droplet size that can be used at each supercooling to measure the rate without having many ice nuclei simultaneously growing. Such a size goes down with supercooling, and for supercooling larger than ~ 50 K, the pressure inside the drop departs from the atmospheric one because of curvature effects (Laplace pressure). When the pressure of the liquid where ice nucleates increases, the nucleation rate decreases, mainly because of an increase of the interfacial free energy.³¹ Taking this into account, we provide simulation estimates of the homogeneous nucleation rate in droplets, and we find good agreement with most droplet-based experimental measurements in a wide supercooling range. The agreement is even better if drops with the radius typically used in the experiments are considered (in this case, a Laplace pressure correction to the rate is noticeable for supercooling larger than 45 K). Such a good agreement has several implications: (i) the data obtained at deep supercooling using nanoscopic drops (blue points in Figure 1) are supported by our simulations, whereas those recently obtained with microscopic drops (downward green triangles in Figure 1) that inspired a fit to the nucleation rate with a maximum at a supercooling of 46 K (dashed pink line in Figure 1) are not; (ii) TIP4P/Ice seems to be a good model to investigate both the thermodynamics and the kinetics of the water-to-ice transition; (iii) the CNT seems to be a solid framework to understand ice nucleation.

AUTHOR INFORMATION

Corresponding Author

*E-mail: esa01@quim.ucm.es.

ORCID

Eduardo Sanz: 0000-0001-6474-5835

Notes

The authors declare no competing financial interest.

ACKNOWLEDGMENTS

This work was funded by grants FIS2013/43209-P and FIS2016/78117-P of the MEC. J.R.E. acknowledges financial support from the FPI grant BES-2014-067625. The authors acknowledge the computer resources and technical assistance provided by the Centro de Supercomputacion y Visualizacion de Madrid (CeSViMa).

REFERENCES

- (1) Cantrell, W.; Heymsfield, A. Production of Ice in Tropospheric Clouds: A Review. *Bull. Am. Meteorol. Soc.* **2005**, *86*, 795–808.
- (2) Baker, M. B. Cloud microphysics and climate. *Science* **1997**, *276*, 1072–1078.
- (3) DeMott, P. J.; Prenni, A. J.; Liu, X.; Kreidenweis, S. M.; Petters, M. D.; Twohy, C. H.; Richardson, M. S.; Eidhammer, T.; Rogers, D. C. Predicting global atmospheric ice nuclei distributions and their impacts on climate. *Proc. Natl. Acad. Sci. U. S. A.* **2010**, *107*, 11217–11222.

- (4) Murray, B. J.; O'Sullivan, D.; Atkinson, J. D.; Webb, M. E. Ice nucleation by particles immersed in supercooled cloud droplets. *Chem. Soc. Rev.* **2012**, *41*, 6519–6554.
- (5) de Boer, G.; Morrison, H.; Shupe, M. D.; Hildner, R. Evidence of liquid dependent ice nucleation in high-latitude stratiform clouds from surface remote sensors. *Geophys. Res. Lett.* **2011**, *38*, L01803.
- (6) Choi, Y.-S.; Lindzen, R. S.; Ho, C.-H.; Kim, J. Space observations of cold-cloud phase change. *Proc. Natl. Acad. Sci. U. S. A.* **2010**, *107*, 11211–11216.
- (7) Westbrook, C. D.; Illingworth, A. J. Evidence that ice forms primarily in supercooled liquid clouds at temperatures $> -27^\circ$ C. *Geophys. Res. Lett.* **2011**, *38*, L14808.
- (8) Rosenfeld, D.; Woodley, W. L. Deep convective clouds with sustained supercooled liquid water down to -37.5° C. *Nature* **2000**, *405*, 440–442.
- (9) Rasmussen, D. H. Ice formation in aqueous systems. *J. Microsc.* **1982**, *128*, 167–174.
- (10) Koop, T.; Luo, B.; Tsias, A.; Peter, T. Water activity as the determinant for homogeneous ice nucleation in aqueous solutions. *Nature* **2000**, *406*, 611–614.
- (11) Turnbull, D. Kinetics of heterogeneous nucleation. *J. Chem. Phys.* **1950**, *18*, 198–203.
- (12) Pruppacher, H. R. A new look at homogeneous ice nucleation in supercooled water drops. *J. Atmos. Sci.* **1995**, *52*, 1924–1933.
- (13) Murray, B. J.; Broadley, S. L.; Wilson, T. W.; Bull, S. J.; Wills, R. H.; Christenson, H. K.; Murray, E. J. Kinetics of the homogeneous freezing of water. *Phys. Chem. Chem. Phys.* **2010**, *12*, 10380.
- (14) Riechers, B.; Wittbracht, F.; Hütten, A.; Koop, T. The homogeneous ice nucleation rate of water droplets produced in a microfluidic device and the role of temperature uncertainty. *Phys. Chem. Chem. Phys.* **2013**, *15*, 5873–5887.
- (15) Stöckel, P.; Weidinger, I. M.; Baumgärtel, H.; Leisner, T. Rates of Homogeneous Ice Nucleation in Levitated H₂O and D₂O Droplets†. *J. Phys. Chem. A* **2005**, *109*, 2540–2546.
- (16) Stan, C. A.; Schneider, G. F.; Shevkoplyas, S. S.; Hashimoto, M.; Ibanescu, M.; Wiley, B. J.; Whitesides, G. M. A microfluidic apparatus for the study of ice nucleation in supercooled water drops. *Lab Chip* **2009**, *9*, 2293–2305.
- (17) Krämer, B.; Hübner, O.; Vortisch, H.; Wöste, L.; Leisner, T.; Schwell, M.; Rühl, E.; Baumgärtel, H. Homogeneous nucleation rates of supercooled water measured in single levitated microdroplets. *J. Chem. Phys.* **1999**, *111*, 6521–6527.
- (18) Duft, D.; Leisner, T. Laboratory evidence for volume-dominated nucleation of ice in supercooled water microdroplets. *Atmos. Chem. Phys.* **2004**, *4*, 1997–2000.
- (19) Rzesanke, D.; Nadolny, J.; Duft, D.; Müller, R.; Kiselev, A.; Leisner, T. On the role of surface charges for homogeneous freezing of supercooled water microdroplets. *Phys. Chem. Chem. Phys.* **2012**, *14*, 9359–9363.
- (20) Benz, S.; Megahed, K.; Möhler, O.; Saathoff, H.; Wagner, R.; Schurath, U. T-dependent rate measurements of homogeneous ice nucleation in cloud droplets using a large atmospheric simulation chamber. *J. Photochem. Photobiol., A* **2005**, *176*, 208–217.
- (21) Manka, A.; Pathak, H.; Tanimura, S.; Wölk, J.; Strey, R.; Wyslouzil, B. E. Freezing water in no-man's land. *Phys. Chem. Chem. Phys.* **2012**, *14*, 4505–4516.
- (22) Huang, J.; Bartell, L. S. Kinetics of Homogeneous Nucleation in the Freezing of Large Water Clusters. *J. Phys. Chem.* **1995**, *99*, 3924–3931.
- (23) Bhabhe, A.; Pathak, H.; Wyslouzil, B. E. Freezing of Heavy Water (D₂O) Nanodroplets. *J. Phys. Chem. A* **2013**, *117*, 5472–5482.
- (24) Amaya, A. J.; Wyslouzil, B. E. Ice nucleation rates near ~ 225 K. *J. Chem. Phys.* **2018**, *148*, 084501.
- (25) Hagen, D. E.; Anderson, R. J.; Kassner, J. L., Jr. Homogeneous condensation-freezing nucleation rate measurements for small water droplets in an expansion cloud chamber. *J. Atmos. Sci.* **1981**, *38*, 1236–1243.
- (26) Laksmono, H.; McQueen, T. A.; Sellberg, J. A.; Loh, N. D.; Huang, C.; Schlesinger, D.; Sierra, R. G.; Hampton, C. Y.; Nordlund,

D.; Beye, M.; et al. Anomalous Behavior of the Homogeneous Ice Nucleation Rate in "No-Man's Land". *J. Phys. Chem. Lett.* **2015**, *6*, 2826–2832.

(27) Koop, T.; Murray, B. J. A physically constrained classical description of the homogeneous nucleation of ice in water. *J. Chem. Phys.* **2016**, *145*, 211915.

(28) Haji-Akbari, A.; Debenedetti, P. G. Perspective: Surface freezing in water: A nexus of experiments and simulations. *J. Chem. Phys.* **2017**, *147*, 060901.

(29) Abascal, J. L. F.; Sanz, E.; Fernandez, R. G.; Vega, C. A potential model for the study of ices and amorphous water: TIP4P/Ice. *J. Chem. Phys.* **2005**, *122*, 234511.

(30) Espinosa, J. R.; Navarro, C.; Sanz, E.; Valeriani, C.; Vega, C. On the time required to freeze water. *J. Chem. Phys.* **2016**, *145*, 211922.

(31) Espinosa, J. R.; Zaragoza, A.; Rosales-Pelaez, P.; Navarro, C.; Valeriani, C.; Vega, C.; Sanz, E. Interfacial free energy as the key to the pressure-induced deceleration of ice nucleation. *Phys. Rev. Lett.* **2016**, *117*, 135702.

(32) Espinosa, J. R.; Vega, C.; Valeriani, C.; Sanz, E. Seeding approach to crystal nucleation. *J. Chem. Phys.* **2016**, *144*, 034501.

(33) Espinosa, J. R.; Vega, C.; Sanz, E. The mold integration method for the calculation of the crystal-fluid interfacial free energy from simulations. *J. Chem. Phys.* **2014**, *141*, 134709.

(34) Xu, Y.; Petrik, N. G.; Smith, R. S.; Kay, B. D.; Kimmel, G. A. Homogeneous nucleation of ice in transiently-heated, supercooled liquid water films. *J. Phys. Chem. Lett.* **2017**, *8*, 5736–5743.

(35) Hrubý, J.; Vinš, V.; Mareš, R.; Hykl, J.; Kalová, J. Surface Tension of Supercooled Water: No Inflection Point down to $-25\text{ }^{\circ}\text{C}$. *J. Phys. Chem. Lett.* **2014**, *5*, 425–428.

(36) Joswiak, M. N.; Do, R.; Doherty, M. F.; Peters, B. Energetic and entropic components of the Tolman length for mW and TIP4P/2005 water nanodroplets. *J. Chem. Phys.* **2016**, *145*, 204703.

(37) Lau, G. V.; Ford, I. J.; Hunt, P. A.; Müller, E. A.; Jackson, G. Surface thermodynamics of planar, cylindrical, and spherical vapour-liquid interfaces of water. *J. Chem. Phys.* **2015**, *142*, 114701.

(38) Lau, G. V.; Hunt, P. A.; Müller, E. A.; Jackson, G.; Ford, I. J. Water droplet excess free energy determined by cluster mitosis using guided molecular dynamics. *J. Chem. Phys.* **2015**, *143*, 244709.

(39) Gibbs, J. W. On the equilibrium of heterogeneous substances. *Trans. Connect. Acad. Sci.* **1876**, *3*, 108–248.

(40) Gibbs, J. W. On the equilibrium of heterogeneous substances. *Trans. Connect. Acad. Sci.* **1878**, *16*, 343–524.

(41) Volmer, M.; Weber, A. Keimbildung in übersättigten Gebilden. *Z. Phys. Chem.* **1926**, *119U*, 277.

(42) Becker, R.; Döring, W. Kinetische Behandlung der Keimbildung in übersättigten Dämpfen. *Ann. Phys.* **1935**, *416*, 719–752.

(43) Frenkel, D.; Smit, B. *Understanding Molecular Simulation*; Academic Press, 2002.

(44) Espinosa, J. R.; Vega, C.; Sanz, E. Ice-Water Interfacial Free Energy for the TIP4P, TIP4P/2005, TIP4P/Ice, and mW Models As Obtained from the Mold Integration Technique. *J. Phys. Chem. C* **2016**, *120*, 8068–8075.

(45) Sanz, E.; Vega, C.; Espinosa, J. R.; Caballero-Bernal, R.; Abascal, J. L. F.; Valeriani, C. Homogeneous ice nucleation at moderate supercooling from molecular simulation. *J. Am. Chem. Soc.* **2013**, *135*, 15008–15017.

(46) Frenkel, D.; Smit, B. *Understanding Molecular Simulation*; Academic Press: London, 1996.

(47) Vega, C.; Sanz, E.; Abascal, J. L. F.; Noya, E. G. Determination of phase diagrams via computer simulation: methodology and applications to water, electrolytes and proteins. *J. Phys.: Condens. Matter* **2008**, *20*, 153101.

(48) Kanno, H.; Speedy, R. J.; Angell, C. A. Supercooling of Water to $-92\text{ }^{\circ}\text{C}$ Under Pressure. *Science* **1975**, *189*, 880–881.